Renewable Energy 267 (2026) 125777

Contents lists available at ScienceDirect

Renewable Energy

journal homepage: www.elsevier.com/locate/renene

State-space modeling and predictive control of wind turbine blade dynamics using ERA-OKID

Satyam Panda [a], Shubham Baisthakur [a], Hamid Reza Karimi [b], Breiffni Fitzgerald [a],*

[a] Department of Civil, Structural and Environmental Engineering, School of Engineering, Trinity College Dublin, Ireland
[b] Department of Mechanical Engineering, Politecnico di Milano, Milan, Italy

ARTICLE INFO

Keywords:
Wind turbine dynamics
State-space modeling
ERA-OKID algorithm
Blade dynamics
Reduced-order modeling

ABSTRACT

This paper presents a robust state-space modeling approach for wind turbine blade dynamics based on the Eigensystem Realization Algorithm (ERA) - Observer/Kalman Filter Identification (OKID) technique. The reduced order model consists of three degrees of freedom for a blade, two flapwise and one edgewise, ensuring accurate dynamic predictions across a wide range of wind speeds. Importantly, the model is derived from a single set of input–output data, thereby avoiding the need for recalibration under different wind conditions. The identified model is embedded within an MPC framework for blade-pitch control. In the above-rated turbulent cases examined here, the controller reduces pitch activity while maintaining satisfactory power regulation. The benefits are most pronounced under higher and/or more turbulent wind conditions, while under lower-wind or less demanding conditions the advantage relative to the baseline becomes less marked. Additionally, the computational efficiency of the model supports its use in large-scale simulations and real-time control applications. The efficacy of the proposed modeling approach is validated through its application to a 15MW offshore wind turbine. The results demonstrate its capability to accurately model blade dynamics efficiently as well as its potential for reliability analysis, fatigue life estimation and wind turbine control system applications.

1. Introduction

As the urgency to combat climate change increases, the energy sector is transitioning toward renewable sources, with wind power playing an increasingly vital role in delivering cleaner energy solutions [1]. Offshore wind energy has gained significant attention due to its potential to generate large amounts of power while incorporating the latest technological advancements that balance high energy density with minimal environmental impact [2]. A current trend in offshore wind development is the deployment of larger turbines to maximize energy capture. However, this also increases structural complexity and operational challenges, necessitating advanced modeling, engineering, and control strategies to ensure reliable performance [3]. Recent studies further underscore design and scaling considerations for modern large turbines, strengthening the case for control-oriented modeling [4]. Addressing these challenges requires effective monitoring and control techniques, such as advanced pitch angle control, which optimizes energy capture while minimizing structural loads and reducing fatigue, particularly under turbulent wind conditions [5].

Data-driven models have become essential tools for accurately representing wind turbine blade dynamics and adapting to varying wind conditions, making them invaluable for a wide range of applications [6, 7]. These models, focused on dynamic adaptability, are particularly essential in managing large wind turbulence and ensuring the structural endurance of turbines. In contrast to traditional methods that focus primarily on steady-state performance, modern approaches prioritize dynamic responses [8]. While capturing the complex dynamics of turbine blades remains a challenge, especially in terms of computational efficiency, these models offer valuable solutions not only for control but also for applications such as reliability [9] and fatigue analysis [10], as well as for scenarios that require real-time outputs such as condition monitoring [11]. In particular, tip-region–aware aerodynamic corrections proposed in [12] help tighten load estimates used by data-driven models. By making large-scale simulations feasible and reducing computational overhead, these models support improved design, performance monitoring, and predictive maintenance strategies across different operational conditions.

In this regard, the field of system identification has become ever more relevant, originally stemming from electrical and mathematical engineering to the study of more complex, multi-input multi-output (MIMO) systems relevant for tasks such as control of wind turbines [13]. System identification originated from the need to build good models for dynamic systems, in order to improve the performance

* Corresponding author.
E-mail address: breiffni.fitzgerald@tcd.ie (B. Fitzgerald).

https://doi.org/10.1016/j.renene.2026.125777
Received 9 July 2025; Received in revised form 7 April 2026; Accepted 10 April 2026
Available online 13 April 2026

of controllers, and it was first developed for SISO (single-input, single-output) systems [14]. Over the years, both the computational power and operational modal analysis have significantly improved system identification methods, which now offer clear advantages, particularly in handling high noise lmomoevels typical of real-world conditions [15]. Such a progression fits perfectly with the requirements of high-fidelity modeling of offshore wind turbine systems to enable the ability to manage highly complex, multi-modal dynamics of very large scale blades subject to variable and often turbulent wind conditions. While machine learning (ML) models have shown promise in various fields, they face challenges such as the need for large amounts of training data, complex feature selection and a lack of transparency in representing the physical dynamics of wind turbines [16]. Alternatively, state-space models provides a more mathematically formulated and structured way to represent turbine blades. They directly capture the physical properties and dynamics of blades, being interpretable and more efficient in obtaining blade inputs [17]. Therefore, state-space models are able to give accurate predictions across a wide variety of conditions with no, or infrequent, need for retraining or recalibration, making them ideal for real-time use in the fast changing offshore environment.

The study of linear system identification emerged in the late 1960s and underwent two parallel development paths that remain dominant in the discipline. The first is the prediction error approach that builds a system model by minimizing the difference between an observed system output and a model-predicted output, often derived under Maximum Likelihood (ML) principle [18]. The second pathway stems from the seminal work of Ho and Kalman on system realization [19,20] which was later generalized by Akaike for output-only identification of systems driven by white noise processes [21]. Maximum likelihood methods yield maximal statistical performance in asymptotic conditions with weakly restrictive assumptions, while subspace-based techniques are preferred due to their computational simplicity and resilience. However, these standard methods face issues for high-dimensionality and highly noisy datasets often found in wind turbine systems.

In the present work, the Eigen-system Realization Algorithm (ERA) is utilized to process the output system response data for the identification of the underlying dynamical system. However, ERA is robust only for output impulse response-based sensing and produces poor prediction results when applied to broad/narrowband type data. This limitation is overcome by integrating Observer Kalman Filter Identification (OKID) with the ERA algorithm. OKID generates an approximately accurate match to the theoretical impulse functions, allowing for effective identification from various types of input data. This unified ERA-OKID framework provides a systematic identification of the system dynamics directly from input/output data, while the iterative nature of OKID ensures that the model adapts to varying wind loads and operational conditions without losing stability. Choosing ERA as the realization algorithm enables this model to retain essential system dynamics while remaining computationally efficient, a critical aspect for applications in large-scale or real-time wind turbine simulations. The ERA-OKID model developed in this work captures three degrees of freedom per blade, two in the flapwise direction and one in the edgewise direction, to represent the primary structural and aerodynamic interactions. These degrees of freedom were selected based on the need to address predominant vibration modes that influence turbine stability and performance, which are directly impacted by pitch angle adjustments. This configuration ensures the model captures essential dynamic characteristics critical for wind turbine stability under varying operational loads.

State-space modeling is crucial in this study, as it provides a concise yet comprehensive representation of the wind turbine's dynamic behavior, capturing essential system characteristics directly from input/output data. Unlike machine learning approaches, which typically require vast amounts of training data and may introduce complexity in feature selection or interpretation, the state-space model derived here is grounded in a clear mathematical structure that reflects the turbine's physical dynamics. This approach leverages well-defined system states, enabling model accuracy across varying conditions without extensive recalibration. Additionally, state-space models streamline applications toward future monitoring/control integration by providing a framework where system stability, responses, and disturbances can be systematically analyzed. This efficiency is particularly valuable in the offshore wind energy context, where real-time adaptability and model accuracy under fluctuating conditions are essential for reliable, low-latency performance and practical applications such as predictive maintenance or control.

The proposed state-space model is employed for blade pitch control using the Model Predictive Control (MPC) framework. Based on predicted blade responses and aerodynamic loads the controller minimizes pitch actuation while maintaining the power output consistency. Motivated by recent progress in predictive control for wind turbines [22], we embed the identified controller-ready model in an MPC framework. Unlike traditional controllers, this approach does not require extensive retuning and is suitable for applications that require both robustness and computational simplicity. Related work on composite blade design/optimization highlights the value of compact, predictive models that interface well with control workflows [23]. Validation on a 15MW offshore wind turbine confirms the efficacy and practicality of the proposed control framework. The results demonstrate its capability to efficiently capture essential blade dynamics, emphasizing its potential in reliability assessments, fatigue evaluations, and optimization of wind turbine control systems.

The main contributions of this work are threefold. First, it applies the ERA-OKID framework to construct a reduced-order state-space model that captures key dynamics of offshore wind turbine blades using only a single input–output dataset, avoiding the need for repeated calibration under different operating conditions. Second, the model captures three principal vibration modes, two in the flapwise and one in the edgewise direction, balancing fidelity with computational efficiency. Third, the model is embedded within an MPC framework that anticipates aerodynamic variations and, in the above-rated turbulent cases examined here, reduces blade-response variability and pitch activity while maintaining satisfactory power regulation.

2. State of the art and research gaps

For large blades, physics-based ROMs commonly use component-mode synthesis (e.g., Craig–Bampton) to reduce FE models while preserving key modal behavior. In parallel, subspace methods identify compact linear state-space models directly from input–output data; in particular, the Eigensystem Realization Algorithm (ERA) and its observer-based prefiltering via OKID (OKID-ERA) are standard tools for controller-ready realizations [24]. For operating turbines, operational modal analysis (OMA) is widely used for output-only identification, and linear parameter-varying (LPV) identification captures operating-point effects (e.g., rotor speed) often together with the multi-blade coordinate (MBC) transform to express rotating dynamics in a fixed frame [25,26].

Beyond gain-scheduled collective-pitch PI, optimal/robust designs (e.g., LQG/LQR) and model predictive control (MPC) address power regulation and fatigue under actuator limits. Individual Pitch Control (IPC) uses MBC-based decoupling to target blade-synchronous loads. Recent work emphasizes explicit trade-offs between load reduction and actuator duty: output-constrained IPC maps the Pareto front on large reference turbines, while constrained subspace predictive repetitive control (cSPRC) achieves notable load cuts at very low duty; importantly, full-scale field tests have demonstrated MPC feasibility on multi-MW machines [27,28]. For fixed-bottom (monopile) and land-based turbines, the dominant baseline architecture remains region-dependent torque control below-rated and a gain-scheduled collective-pitch PI loop above-rated; recent NREL updates document modern scheduling practices and their implementation with OpenFAST linearization workflows [29]. Open-source controllers such as ROSCO operationalize these principles for both fixed and floating platforms and are now widely used for reference turbines (including NREL 5-MW and IEA 15-MW) [30]. For load mitigation on large fixed-bottom offshore turbines, IPC and related blade-synchronous strategies continue to be actively developed and validated, including recent tuned IPC studies on large fixed-bottom offshore reference models [22]. Beyond classical gain scheduling, LPV control provides a systematic framework to guarantee performance across operating regions, including designs spanning partial- and full-load trajectories [31].

This work pursues a controller-ready identification-to-control pathway: (i) a single-dataset ERA–OKID procedure yields a compact linear state-space model; (ii) in our tests, the same identified model remained usable across the examined above-rated wind speeds without re-identification or LPV scheduling. The results suggest that, for these tested turbulent cases, meaningful load mitigation can be achieved without increased pitch activity; and (iii) it integrates directly with MPC at modest online cost. This contrasts with CMS/POD/ML surrogates that often require curated multi-condition datasets and extra steps to become controller-ready, with OMA which is output-only, and with LPV/GS approaches that need explicit scheduling and multiple linearizations. In the broader control context, our results fall within the low-actuation, load-reducing regime highlighted by recent output-constrained IPC and validated by field MPC studies, indicating that effective load mitigation does not require increased pitch activity.

3. Numerical model of IEA-15MW reference wind turbine

This study utilizes the specifications of the International Energy Agency (IEA) 15MW wind turbine, an IEC Class 1B direct-drive system featuring a 240-meter rotor diameter and a hub height of 150 m [32]. The key design and operational parameters of this wind turbine, are thoroughly documented in our previous work [7]. The validation results, which demonstrates a good agreement between OpenFAST and the numerical model, are also reported in the literature [7].

The dynamic model of this wind turbine is formulated using Kane's method [33], which makes it easier to obtain equations of motion and implement them into computational models. Compared to conventional formulations such as the Euler–Lagrange approach and D'Alembert principle, Kane's formulation significantly simplifies the derivations. This method is highly beneficial for the assessment of multi–body dynamic systems, in which many interconnected components create an assemblage. The equations for equilibria of a simple holonomic multi-body system, obtained through the application of Kane's methodology are given by:

$$F_r + F_r^* = 0 \tag{1}$$

where F_r denotes the generalized active forces, and F_r^* represents the generalized inertia forces. These forces can be expressed in terms of kinematic quantities as follows:

$$F_r = \sum_{i=1}^{n} {}^E v_r^{X_i} \cdot F^{X_i} + {}^E \omega_r^{N_i} \cdot M^{N_i} \tag{2}$$

and,

$$F_r^* = -\sum_{i=1}^{n} {}^E v_r^{X_i} (m^{N_i}\, {}^E a^{X_i}) - {}^E \omega_r^{N_i} \cdot {}^E \dot{H}^{N_i} \tag{3}$$

The force vector acting on the point X_i is denoted by F^{X_i}, while M^{N_i} represents the moment vector on the rigid body N_i. The partial linear velocity of X_i and the partial angular velocity of N_i in the inertial frame are expressed as ${}^E v_r^{X_i}$ and ${}^E \omega_r^{N_i}$, respectively. The time derivative of the angular momentum of the rigid body N_i, about its center of mass X_i in the inertial frame, is represented as ${}^E \dot{H}^{N_i}$ and can be computed using the following equation:

$${}^E \dot{H}^{N_i} = \bar{\bar{I}}^{N_i} \cdot {}^E \alpha^{N_i} + {}^E \omega^{N_i} \times \bar{\bar{I}}^{N_i} \cdot {}^E \omega^{N_i} \tag{4}$$

In this work, three degrees of freedom per blade are considered, representing first two flapwise modes and the first edgewise mode. The blades are represented as flexible members by the modal summation method [7], which allows the representation of their dynamic behavior through a combination of mode shapes and modal coordinates. The coupled vibration modes for these blades are derived using BModes [34], which is a tool for calculating the natural frequencies in flexible structures subject to rotation and other external forces. The equations of motion for the blade dynamics are expressed in the general form:

$$M(q,t)\ddot{q} + f(q,\dot{q},t) = 0 \tag{5}$$

where, $M(q,t)$ is the inertia matrix corresponding to the blade dynamics, $\ddot{q}$ being the acceleration vector and $f(q,\dot{q},t)$ is the force vector comprising of external and restoring forces acting on structure. The nonlinear equations of motion are linearized into a state-space representation to allow efficient analysis and controller design. In this methodology, the state-space matrices are obtained by integrating a data-driven approach with some physics knowledge of the system. Using the system responses calculated from input–output data along with available knowledge about the physical dynamics (like flexible blade modes and aerodynamic interactions) allows our method to realize a state-space representation that captures the true behavior of the system. In this study, the ERA-OKID method, a direct input–output identification algorithm, is employed to develop a state-space model without the need to explicitly derive physical parameters. This approach produces a compact, control-oriented model suitable for advanced applications such as Model Predictive Control (MPC), enabling near-optimal performance across a wide range of operating conditions. Beyond control, the model's computational efficiency makes it particularly valuable for simulation-intensive tasks, including fatigue and reliability analysis, as well as applications requiring real-time implementation.

4. Development of state space model

The mathematical formulation and the underlying concepts of the Eigen-system Realization Algorithm (ERA) and Observer Kalman Filter Identification (OKID) are discussed in detail. The discrete-time LTI state-space model used throughout this section is

$$\begin{aligned} x(i+1) &= Ax(i) + Bu(i) \\ y(i) &= Cx(i) + Du(i) \end{aligned} \tag{6}$$

where, $x(i) \in \mathbb{R}^n$ corresponds to the system states, $y(i) \in \mathbb{R}^q$ is the system output. $u(i) \in \mathbb{R}^m$ denotes the input. Here, n denotes the identified model order (singular values of the Hankel matrix), while m and q denote the numbers of inputs and outputs, respectively. In this work, the input $u(i)$ is constructed as an effective generalized aerodynamic excitation obtained by a weighted modal summation of the distributed aerodynamic forces evaluated at the blade nodes along the span (consistent with the modal-summation blade representation described in Section 3). This reduces the distributed forcing to a compact input suitable for identification while retaining the dominant spanwise loading contribution. The outputs are chosen to represent the dominant blade motion relevant to monitoring and control. Specifically, the output vector $y(i)$ correspond to the first three blade dynamic components considered in this study (two flapwise and one edgewise), expressed in terms of blade-tip vibration responses. Finally, the state $x(i)$ is the internal realization state of the identified reduced-order model.

4.1. Eigen-system realization algorithm (ERA)

The Eigen-system Realization Algorithm (ERA), introduced in 1985 by Juang and Pappa [24], is an extension of Ho and Kalman's realization method [19]. Designed for use in the time domain, ERA is essential for simplifying dynamic system models and identifying modal parameters. It operates by deriving the system's state-space matrices

$\left(A_d, B_d, C\right)$ for linear time-invariant (LTI) systems, based on their impulse response. In the discrete LTI model, an impulse input is defined with $u(0) = 1$ and $u(k) = 0$ for $k = 1, 2, \ldots, p$. This impulse triggers responses, known as Markov parameters [20], which are represented as follows:

$$\begin{aligned} &Z(0) = D \\ &Z(1) = CB_d \\ &Z(2) = CA_d^1 B_d \\ &\quad\vdots \\ &Z(k) = CA_d^{k-1} B_d \end{aligned} \tag{7}$$

The embedded system matrices A_d, B_d, C, and D are derived from the Markov parameters. The process initiates by constructing a Hankel matrix, or alternatively, a shifted Hankel matrix [35], as expressed in Eq. (8). This matrix formulation is central to the ERA algorithm, enabling the extraction of the system matrices essential for model representation.

$$\mathcal{H}(k-1) = \begin{bmatrix} Z(k) & Z(k+1) & \cdots & Z(k+p) \\ Z(k+1) & Z(k+2) & \cdots & Z(k+p+1) \\ \vdots & \vdots & \cdots & \vdots \\ Z(k+p) & Z(k+p+1) & \cdots & Z(k+2p-1) \end{bmatrix} \tag{8}$$

and for $k = 1$ and 2,

$$\begin{aligned} &\underbrace{\mathcal{H}(0) = \begin{bmatrix} Z(1) & Z(2) & \cdots & Z(p+1) \\ Z(2) & Z(3) & \cdots & Z(p+2) \\ \vdots & \vdots & \cdots & \vdots \\ Z(p+1) & Z(p+2) & \cdots & Z(2p) \end{bmatrix}}_{\text{hankel matrix}}; \\ &\underbrace{\mathcal{H}(1) = \begin{bmatrix} Z(2) & Z(3) & \cdots & Z(p+2) \\ Z(3) & Z(4) & \cdots & Z(p+3) \\ \vdots & \vdots & \cdots & \vdots \\ Z(p+2) & Z(p+3) & \cdots & Z(2p+1) \end{bmatrix}}_{\text{shifted hankel matrix}} \end{aligned} \tag{9}$$

Substituting the Markov parameters in the above equation for $\mathcal{H}(0)$ and decomposing it into two matrices,

$$\begin{aligned} \mathcal{H}(0) &= \begin{bmatrix} CB_d & CA_d^1 B_d & \cdots & CA_d^{p-1} B_d \\ CA_d^1 B_d & CA_d^2 B_d & \cdots & CA_d^p B_d \\ \vdots & \vdots & \cdots & \vdots \\ CA_d^{p-1} B_d & CA_d^p B_d & \cdots & CA_d^{2p-1} B_d \end{bmatrix} \\ \mathcal{H}(0) &= O_p C_p \end{aligned} \tag{10}$$

where C_p and O_p are controllability and observability matrices, respectively, defined as:

$$C_p = \begin{bmatrix} A_d^{p-1} B_d & \ldots & A_d B_d & B_d \end{bmatrix} \quad O_p = \begin{bmatrix} C \\ CA_d \\ \vdots \\ CA_d^{p-1} \end{bmatrix} \tag{11}$$

The dynamical system of order n is considered to be both controllable and observable such that the rank of the matrices C_p and O_p are n. Therefore, according to Eq. (10), the rank of the matrix $\mathcal{H}(0)$ is n. The factorization of $\mathcal{H}(0)$ using singular value decomposition (SVD) leads to the matrices P, V, Q such that,

$$\mathcal{H}(0) = PVQ^T \tag{12}$$

where P, Q are orthonormal matrices and V is a singular diagonal matrix given by,

$$V = \begin{bmatrix} S_n & 0 \\ 0 & 0 \end{bmatrix} \tag{13}$$

where, $S_n = diag\left[\sigma_1, \sigma_2, \ldots, \sigma_i, \sigma_{i+1}, \ldots, \sigma_n\right]$ with $\sigma_1 \geq \sigma_2 \geq \ldots \sigma_n \geq 0$ and 0's corresponds to the zero matrices of appropriate dimensions. Consider the truncated versions of the matrices P and Q as P_n and Q_n such that P_n and Q_n are formed by the first n columns of P and Q respectively. Accordingly, Eq. (12) is revised as,

$$\mathcal{H}(0) = P_n S_n Q_n^T \tag{14}$$

Since S_n is a positive real diagonal matrix, it can be expressed as, $S_n = S_n^{\frac{1}{2}} S_n^{\frac{1}{2}}$. Substituting the value of S_n in Eq. (14) and comparing it with Eq. (10), the following relationship is obtained:

$$\begin{aligned} &\mathcal{H}(0) = \left[P_n S_n^{\frac{1}{2}}\right]\left[S_n^{\frac{1}{2}} Q_n^T\right] \cong O_p C_p \\ &\therefore O_p = P_n S_n^{\frac{1}{2}}; \quad C_p = S_n^{\frac{1}{2}} Q_n^T \end{aligned} \tag{15}$$

The above choice for selecting the controllability and observability matrices is valid in a sense that,

$$\begin{aligned} &O_p^T O_p = S_n^{\frac{1}{2}} P_n^T P_n S_n^{\frac{1}{2}} = S_n \\ &C_p C_p^T = S_n^{\frac{1}{2}} Q_n^T Q_n S_n^{\frac{1}{2}} = S_n \end{aligned} \tag{16}$$

Further from Eq. (8),

$$\begin{aligned} &\mathcal{H}(k-1) = \begin{bmatrix} CA^{k-1} B_d & CA_d^k B_d & \cdots & CA_d^{k+p-1} B_d \\ CA_d^k B_d & CA_d^{k+1} B_d & \cdots & CA_d^{k+p} B_d \\ \vdots & \vdots & \cdots & \vdots \\ CA_d^{k+p-1} B_d & CA_d^{k+p} B_d & \cdots & CA_d^{k+2p-1} B_d \end{bmatrix} \\ &\Rightarrow \mathcal{H}(k-1) = O_p A_d^{k-1} C_p \end{aligned} \tag{17}$$

For $k = 2$, $\mathcal{H}(1) = O_p A_d C_p = P_n S_n^{\frac{1}{2}} A_d S_n^{\frac{1}{2}} Q_n^T$. $\therefore$ the system matrix is given as,

$$A_d = S_n^{-\frac{1}{2}} P_n^T \mathcal{H}(1) Q_n S_n^{-\frac{1}{2}}. \tag{18}$$

After determining A_d, the matrices B_d, C and D can be determined as the first s rows of C_p and the first r rows of O_p, respectively, by the following operations:

$$\begin{aligned} &B_d = C_p \begin{bmatrix} I_{s\times s} & 0 & \ldots & 0 \end{bmatrix}^T \\ &C = \begin{bmatrix} I_{r\times r} & 0 & \ldots & 0 \end{bmatrix} O_p \\ &D = Z(0) \end{aligned} \tag{19}$$

In civil engineering, the Eigensystem Realization Algorithm (ERA) is frequently adopted to identify lightly damped structures but its application is restricted due to the need for pure free or impulse response measurements which are often impractical because of structural dimensions, safety restrictions or ambient vibrations [36]. However, state-space models are indispensable for estimation, filtering and control design which has motivated growing interest in identifying these models directly from input–output data. As reported in [36], among existing methods subspace methods are advantageous since they are robust, non-iterative and do not need a specific parameterization to fit MIMO systems.

4.2. Observer/Kalman filter identification (OKID)

The Observer/Kalman Filter Identification (OKID) algorithm is a popular method for deriving state-space models [37]. For this, it estimates the Markov parameters of a Kalman filter using ordinary least squares (OLS) from distinguishable samples, and then generates the process Markov parameters. Lastly, ERA is used to obtain the state-space modeling. Such a combination benefits from the efficient linear algebra routines available while obtaining both accurate and fast results.

Assuming zero initial conditions i.e. $x(0) = 0$, Eq. (6) can be written as:

$$y_{q\times l} = \mathbf{Z}_{q\times ml} \mathbf{U}_{ml\times l} \tag{20}$$

where, y, Z and U are given as,

$$\mathbf{U} = \begin{bmatrix} u(0) & u(1) & u(2) & \dots & u(l-1) \\ & u(0) & u(1) & \dots & u(l-2) \\ & & u(0) & \dots & u(l-3) \\ & & & \ddots & \vdots \\ & & & & u(0) \end{bmatrix}$$
$$\mathbf{Z} = \begin{bmatrix} D & CB & CAB & \dots & CA^{l-2}B \end{bmatrix} \tag{21}$$

Here, m is the number of inputs, q denotes the number of outputs and l corresponds to the number of data samples. The Markov parameters in the matrix $\mathbf{Z}$ can be computed as: $\mathbf{Z} = y\mathbf{U}^{-1}$. However, from Eq. (20), it can be observed that $\mathbf{Z}$ contains $q \times ml$ unknowns with only $q \times l$ equations. Therefore, $\mathbf{Z}$ cannot be accurately computed. Consider p to be sufficiently large such that A is asymptotically stable i.e. $A^i \approx 0$, $\forall i \geq p$. Therefore, with the truncated versions of $\mathbf{Z}$ and $\mathbf{U}$, Eq. (20) can be revised as:

$$y_{q\times l} \approx Z_{q\times mp} U_{mp\times l} \tag{22}$$

where, the truncated $U\,[m(p+1)\times l]$ and $Z\,[q \times m(p+1)]$ are given as:

$$y = \begin{bmatrix} y(0) & y(1) & y(2) & \dots & y(p) & \dots & y(l-1) \end{bmatrix}$$
$$Z = \begin{bmatrix} D & CB & CAB & \dots & CA^{p-1}B \end{bmatrix}$$
$$U = \begin{bmatrix} u(0) & u(1) & u(2) & \dots & u(p) & \dots & u(l-1) \\ & u(0) & u(1) & \dots & u(p-1) & \dots & u(l-2) \\ & & u(0) & \dots & u(p-2) & \dots & u(l-3) \\ & & & \ddots & \vdots & \dots & \vdots \\ & & & & u(0) & \dots & u(l-p-1) \end{bmatrix} \tag{23}$$

The data length l is chosen such that it is greater than $m(p+1)$ and p is chosen such that for $i \geq p$, $CA^iB \approx 0$. From Eq. (22) it is observed that the number of equations ($q \times l$) are more than the unknowns ($q \times m(p+1)$). Therefore, the first p Markov parameters are approximated by $Z = yU^+$, where, U^+ is the pseudoinverse of U and the approximation error decreases as the value of p increases. It is to be noted that for lightly damped structures, the required value of p and l are quite large to approximate the Markov parameters using Eq. (22) which renders numerical inefficiency to the computation of the pseudoinverse of U. In order to account for this, consider the algebraic manipulation as follows,

$$\begin{aligned} x(i+1) &= Ax(i) + Bu(i) + My(i) - My(i) \\ &= (A+MC)x(i) + (B+MD)u(i) - My(i) \\ &= \bar{A}x(i) + \bar{B}v(i) \\ y(i) &= Cx(i) + Du(i) \end{aligned} \tag{24}$$

where,

$$\begin{aligned} \bar{A} &= A + MC \\ \bar{B} &= \begin{bmatrix} B+MD, & -M \end{bmatrix} \\ v(i) &= \begin{bmatrix} u(i) \\ y(i) \end{bmatrix} \end{aligned} \tag{25}$$

Here, the gain matrix M is introduced which is of size $n \times q$ and it is chosen in order to stabilize the matrix $\bar{A}$. If $x(i)$ is considered to be an observer state, then Eq. (24) is an observer equation with Markov parameters referred to as observer Markov parameters. For Eq. (24), the input–output relationship can be described as:

$$y_{q\times l} = \bar{\mathbf{Z}}_{q\times[(q+m)(l-1)+m]} \mathbf{V}_{[(q+m)(l-1)+m]\times l} \tag{26}$$

where, $\bar{\mathbf{Z}}$ and $\mathbf{V}$ are given as,

$$\bar{\mathbf{Z}} = \begin{bmatrix} D & C\bar{B} & C\bar{A}\bar{B} & \dots & C\bar{A}^{l-2}\bar{B} \end{bmatrix}$$
$$\mathbf{V} = \begin{bmatrix} u(0) & u(1) & u(2) & \dots & u(p) & \dots & u(l-1) \\ & v(0) & v(1) & \dots & v(p-1) & \dots & v(l-2) \\ & & v(0) & \dots & v(p-2) & \dots & v(l-3) \\ & & & \ddots & \vdots & \dots & \vdots \\ & & & & v(0) & \dots & v(l-p-1) \\ & & & & & \ddots & \vdots \\ & & & & & & v(0) \end{bmatrix} \tag{27}$$

Similar to the calculations in Eq. (22), considering the integer p to be sufficiently large such that for $i \geq p$, $C\bar{A}^i\bar{B} \approx 0$, the observer Markov parameters in Eq. (26) can be computed by considering the following truncated version,

$$y_{q\times l} = \bar{Z}_{q\times[(q+m)p+m]} V_{[(q+m)p+m]\times l} \tag{28}$$

where,

$$\bar{\mathbf{Z}} = \begin{bmatrix} D & C\bar{B} & C\bar{A}\bar{B} & \dots & C\bar{A}^{p-1}\bar{B} \end{bmatrix}$$
$$\mathbf{V} = \begin{bmatrix} u(0) & u(1) & u(2) & \dots & u(p) & \dots & u(l-1) \\ & v(0) & v(1) & \dots & v(p-1) & \dots & v(l-2) \\ & & v(0) & \dots & v(p-2) & \dots & v(l-3) \\ & & & \ddots & \vdots & \dots & \vdots \\ & & & & v(0) & \dots & v(l-p-1) \end{bmatrix} \tag{29}$$

Using Eq. (28), the first p observer Markov parameters can be obtained by $\bar{Z} = yV^+$ (+ denotes the pseudoinverse). Although the approximated Markov parameters may not decay during the first $p-1$ steps, yet for $i \geq p$, they yield $C\bar{A}^i\bar{B} \approx 0$ and noise-free data. All these formulations considered zero initial conditions. However, for non-zero unknown initial conditions, considering $\bar{A}^p$ to be sufficiently small, Eq. (28) is modified by deleting the first p columns as:

$$\bar{y} = \bar{Z}\bar{V} \tag{30}$$

where,

$$\bar{y} = \begin{bmatrix} y(p) & y(p+1) & y(p+2) & \dots & y(l-1) \end{bmatrix}$$
$$\bar{V} = \begin{bmatrix} u(p) & u(p+1) & \dots & u(l-1) \\ v(p-1) & v(p) & \dots & v(l-2) \\ v(p-2) & v(p-1) & \dots & v(l-3) \\ \vdots & \vdots & \vdots & \ddots \\ v(0) & v(1) & \dots & v(l-p-1) \end{bmatrix} \tag{31}$$

The observer Markov parameters are identified through a least square solution of Eq. (30), which yields $\bar{Z} = \bar{y}\bar{V}^T\left[\bar{V}\bar{V}^T\right]^{-1}$, provided $\left[\bar{V}\bar{V}^T\right]^{-1}$ exists, otherwise $\bar{V}^T\left[\bar{V}\bar{V}^T\right]^{-1}$ is replaced by $\bar{V}^T$.

4.2.1. Identification of actual Markov parameters and observer gain

To derive the system Markov parameters, Z from the identified observer Markov parameters, $\bar{Z}$, consider the following partition,

$$\bar{Z} = \begin{bmatrix} \bar{Z}_{-1} & \bar{Z}_0 & \bar{Z}_1 & \dots & \bar{Z}_{p-1} \end{bmatrix} \tag{32}$$

where,

$$\begin{aligned} \bar{Z}_k &= C\bar{A}^k\bar{B} \\ &= \left[\bar{Y}_k^{(1)}, \bar{Y}_k^{(2)}\right]; \quad k = 0, 1, 2, \dots \quad \text{and} \quad \bar{Z}_{-1} = D \end{aligned} \tag{33}$$

The system Markov parameters Y_k for $k = 0, 1, 2, \dots$ can be expressed in terms of the observer Markov parameters as:

$$Y_k = \bar{Y}_k^{(1)} + \sum_{i=0}^{k-1} \bar{Y}_i^{(2)} Z_{k-i-1} + \bar{Y}_k^{(2)} D, \tag{34}$$

where: $\bar{Y}_k^{(1)} = C(A+MC)^k(B+MD)$, $\bar{Y}_i^{(2)} Z_{k-i-1}$ represents interactions between previous observer and system Markov parameters and $\bar{Y}_k^{(2)} D$ accounts for direct contributions from the disturbance D. Thus, the actual system parameters are obtained from the $p+1$ observer Markov parameters computed as a least squares solution of Eq. (28). The integer p is chosen to be sufficiently large such that $\bar{Y}_k^{(1)}$ and $\bar{Y}_k^{(2)} \approx 0$ for $k > p$. Eq. (34) can be re-written in the matrix form as:

$$\begin{bmatrix} I & & & \\ -\bar{Y}_0^{(2)} & I & & \\ -\bar{Y}_1^{(2)} & -\bar{Y}_0^{(2)} & \ddots & \\ \vdots & \vdots & & \\ -\bar{Z}_{k-1}^{(2)} & -\bar{Z}_{k-2}^{(2)} & \dots & I \end{bmatrix} \begin{bmatrix} Y_0 \\ Y_1 \\ Y_2 \\ \vdots \\ Y_k \end{bmatrix} = \begin{bmatrix} \bar{Y}_0^{(1)} + \bar{Y}_0^{(2)} D \\ \bar{Y}_1^{(1)} + \bar{Y}_1^{(2)} D \\ \bar{Y}_2^{(1)} + \bar{Y}_2^{(2)} D \\ \vdots \\ \bar{Y}_k^{(1)} + \bar{Y}_k^{(2)} D \end{bmatrix} \tag{35}$$

Here, I and $\bar{Y}_i^{(2)}$ $(i = 0, 1, 2, \dots, k)$ are $q \times q$ square matrices. In order to identify the observer gain M, the sequence of parameters are first recovered in terms of the observer Markov parameters.

$$Y_k^0 = CA^k M \qquad k = 0, 1, 2, \dots \tag{36}$$

The parameters in this sequence are obtained as follows:

$$\begin{aligned} Y_0^0 &= CM = -\bar{Z}_0^{(2)} \\ Y_1^0 &= CAM = C\left(\bar{A} - MC\right) M = -\bar{Z}_1^{(2)} + \bar{Z}_0^{(2)} Y_0^0 \end{aligned} \tag{37}$$

Repeating similar calculations for Y_k^0, the general relationship is given as,

$$Y_k^0 = -\bar{Y}_k^{(2)} + \sum_{i=0}^{k-1} \bar{Y}_i^{(2)} Z_{k-i-1}^0 \tag{38}$$

Once the sequence Y_0^k is obtained, the system matrices A and C can be identified using ERA algorithm from the system Markov parameter sequence, Y_k derived in Eq. (34). To compute the observer gain, M consider the following equation,

$$M = \left(O^T O\right)^{-1} O^T Y^0 \tag{39}$$

where, the matrices O and Z^0 are given as,

$$O = \begin{bmatrix} C \\ CA \\ CA^2 \\ \vdots \\ CA^k \end{bmatrix}, \quad Z^0 = \begin{bmatrix} Y_0^0 \\ Y_1^0 \\ Y_2^0 \\ \vdots \\ Y_k^0 \end{bmatrix} = \begin{bmatrix} CM \\ CAM \\ CA^2M \\ \vdots \\ CA^kM \end{bmatrix} \tag{40}$$

Now Eq. (38) can be written in the matrix form as,

$$\begin{bmatrix} I & & & & \\ -\bar{Y}_0^{(2)} & I & & & \\ -\bar{Y}_1^{(2)} & -\bar{Y}_0^{(2)} & I & & \\ \vdots & \vdots & \vdots & \ddots & \\ -\bar{Z}_{k-1}^{(2)} & -\bar{Z}_{k-2}^{(2)} & -\bar{Z}_{k-3}^{(2)} & \dots & I \end{bmatrix} \begin{bmatrix} Y_0^0 \\ Y_1^0 \\ Y_2^0 \\ \vdots \\ Y_k^0 \end{bmatrix} = \begin{bmatrix} -\bar{Y}_0^{(2)} \\ -\bar{Y}_1^{(2)} \\ -\bar{Y}_2^{(2)} \\ \vdots \\ -\bar{Y}_k^{(2)} \end{bmatrix} \tag{41}$$

The observer gain M in Eq. (39) is identified uniquely from the observer gain Markov parameters. The system Markov parameters in Eq. (34) and the observer gain Markov parameters in Eq. (38) can be clubbed into a single matrix equation to solve for Y_k and $Z(k^0)$, simultaneously, as follows:

$$\begin{aligned} P_k &= \begin{bmatrix} Y_k & Y_k^0 \end{bmatrix} = \begin{bmatrix} CA^kB & CA^kM \end{bmatrix} \\ &= \begin{bmatrix} \bar{Y}_k^{(1)} + \bar{Y}_k^{(2)} D & -\bar{Y}_k^{(2)} \end{bmatrix} \\ &\quad + \sum_{i=0}^{k-1} \bar{Y}_i^{(2)} \begin{bmatrix} Z_{k-i-1} & Z_{k-i-1}^0 \end{bmatrix} \end{aligned} \tag{42}$$

In the OKID algorithm, P_k is used in a Hankel matrix to identify the system matrices, A, B, C and D and the observer gain M by employing ERA technique. The framework for the ERA-OKID algorithm is presented the Algorithm 1 and a graphical abstract is shown in Fig. 1.

Algorithm 1 Combined OKID-ERA Algorithm

OKID Stage:
Input: Time-series data x_k ▷ Refer Eq. (6) for the system state-space model
Choose a sufficiently large integer p ▷ Stability assumption for A^i in Eq. (22)
Solve for the truncated input-output relationship ▷ Refer Eq. (22)
Compute observer Markov parameters $\bar{Z}$ ▷ See Eq. (28)
Use least squares to approximate $\bar{Z}$ ▷ Refer Eq. (30)
Derive system Markov parameters Y_k from $\bar{Z}$ ▷ Refer Eq. (34)
Derive observer gain Markov parameters Y_k^0 ▷ Refer Eq. (38)
Compute observer gain M ▷ Refer Eq. (39)
ERA Stage:
Input: System Markov parameters Y_k
Construct the Hankel matrix $\mathcal{H}(0)$ ▷ Refer Eq. (8)
Perform Singular Value Decomposition (SVD) on $\mathcal{H}(0)$: $\mathcal{H}(0) = PSQ^T$ ▷ Refer Eq. (12)
Compute observability (O_p) and controllability (C_p) matrices ▷ Refer Eq. (15)
Form the shifted Hankel matrix $\mathcal{H}(1)$ and compute A_d ▷ Refer Eq. (18)
Derive the matrices B_d, C, and D ▷ Refer Eq. (19)
Output:
Identified state-space model $[A, B, C, D]$

4.3. Results and discussions

This section validates and analyzes the state-space model developed in diagnostics using the ERA-OKID with its ability to describe wind turbine dynamics at different operational conditions on a 15MW offshore wind turbine. The ERA-OKID method creates a state-space model from only a single input/output pair which is one of its major merits, because in many real situations several input/output data or calibration steps are not easily achievable. Thereafter, it was validated using real wind speed profiles, making it relevant to offshore operational conditions. We focused on modeling the wind turbine blades, specifically capturing their dynamic response to aerodynamic forces and structural interactions. The blades were modeled to include three modes, representing two degrees of freedom in the flapwise direction and one degree of freedom in the edgewise direction. These modes account for the primary deformation patterns under varying wind loads, thus reflecting the blade's physical response under real-world operating conditions. In order to describe the blade dynamics in the state-space form, input and output data are needed to identify the model. The system input is defined as a weighted modal summation of the aerodynamic forces, specified at 50 nodal points per blade, integrated across the blade span. The present approach approximating the distributed forces along the blade as a single modal input guarantees that the spatial variability of aerodynamic forces are well captured in the modeling framework. The reference output data is the vibration responses at the blade tip and physical responses with respect to the three modes defined for the model. High-fidelity input–output data used for ERA–OKID identification are generated using OpenFAST with the full turbine model, with ElastoDyn structural DOFs enabled (set to TRUE). The reduced-order identification then uses only the selected blade-response outputs (two flapwise and one edgewise response channels) extracted from these simulations. This output selection is vital to accurately represent the behavior of the system, since the tip response reveals the key aspects of the overall dynamics of the blade under variable aerodynamic loads. The model identification process involves first applying the Observer/Kalman Filter Identification (OKID) technique to estimate the observer Markov parameters. OKID is particularly useful here as it allows the extraction of these parameters from noisy data while preserving the physical realism of the system response. By treating

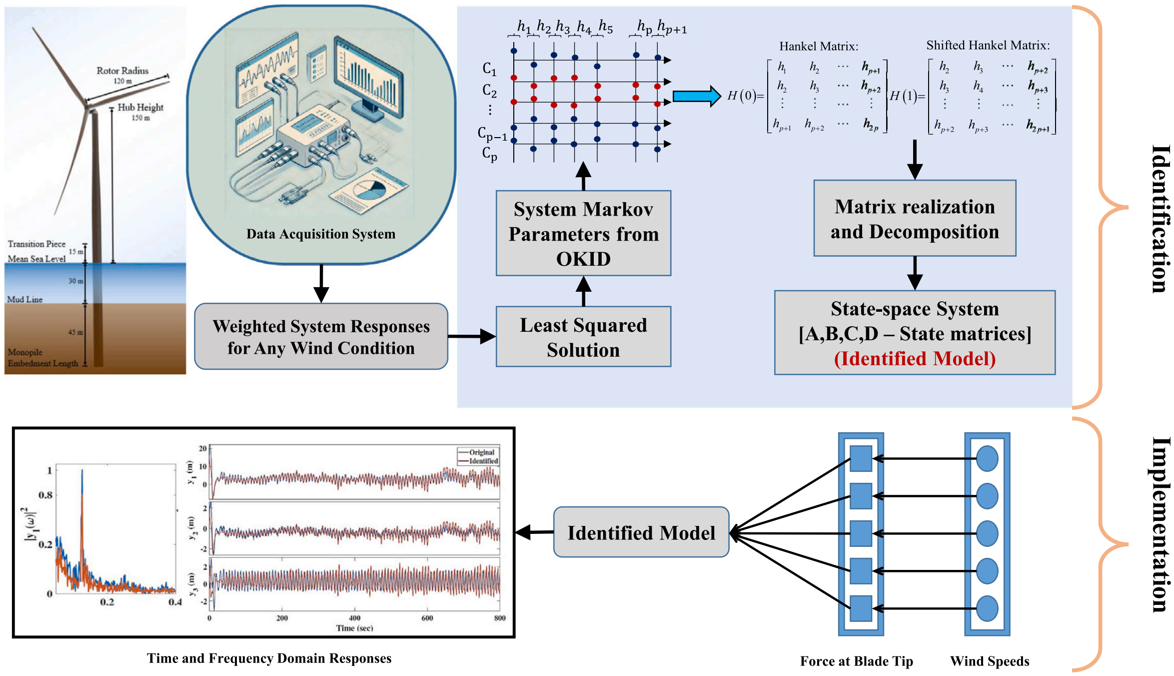

Fig. 1. Identification of state-space models for wind turbine blades using ERA-OKID algorithm.

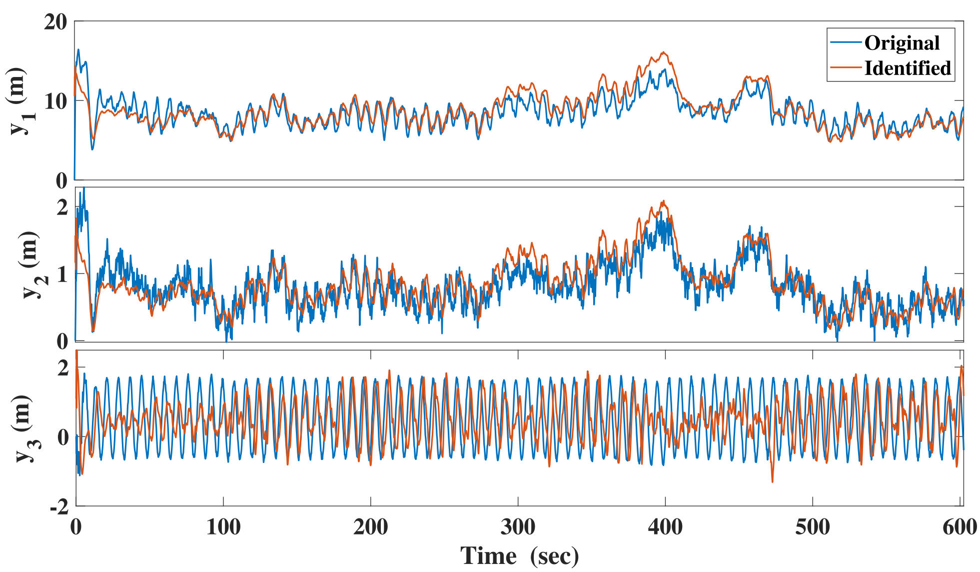

Fig. 2. Comparison of original (OpenFAST full-order simulation) and identified blade tip deformation of 15MW offshore wind turbine under turbulent wind conditions at 12.4046 m/s.

the blade tip responses as outputs and the weighted modal forces as inputs, OKID enables the estimation of system behavior under ambient and forced vibration conditions, which are typical in an offshore environment. Following the OKID estimation, the Eigensystem Realization Algorithm (ERA) is applied to the computed Markov parameters. ERA transforms these parameters into a reduced-order state-space model that accurately represents the essential dynamic characteristics of the turbine blade system. This reduced model, derived from a single input/output dataset, provides a computationally efficient yet robust representation of the blade dynamics, supporting future applications in control, diagnostics, and performance monitoring of offshore wind turbines.

We derive the state-space model for a single wind speed 12.4046 m/s and apply it at multiple wind speeds. This wind speed was chosen as it captures significant dynamic behavior without entering saturation or cut-out conditions. While the model is identified at this specific point, we investigate its performance across a range of wind speeds to assess its robustness under varying turbulent conditions. The means (μ) and standard deviations (σ) of blade tip deformation varies with wind speed as there are differences in turbulence intensity and aerodynamic conditions naturally. We account for this variability by extracting the normalized response, or z-factor, using the equation: $y = \mu + \sigma z$, where y is the blade tip deformation, and μ and σ are mean and standard deviation respectively. Here, the normalization removes deviation of mean and variance between conditions to create a consistency at different wind states. For each wind speed, μ and σ are pre-computed as shown in Table 1. When turbulence levels are different, these quantities do not vary drastically at identical wind speeds enabling successful and confident application of the model. These values of μ and σ are subsequently embedded with the z-factor, enabling the identification

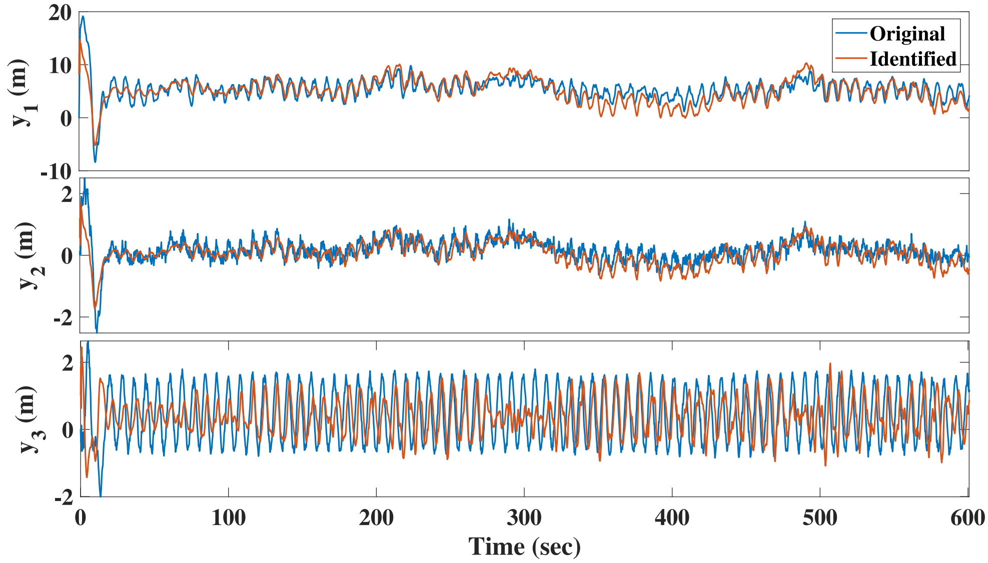

Fig. 3. Comparison of original (OpenFAST full-order simulation) and identified blade tip deformation of 15MW offshore wind turbine under turbulent wind conditions at 15.2094 m/s.

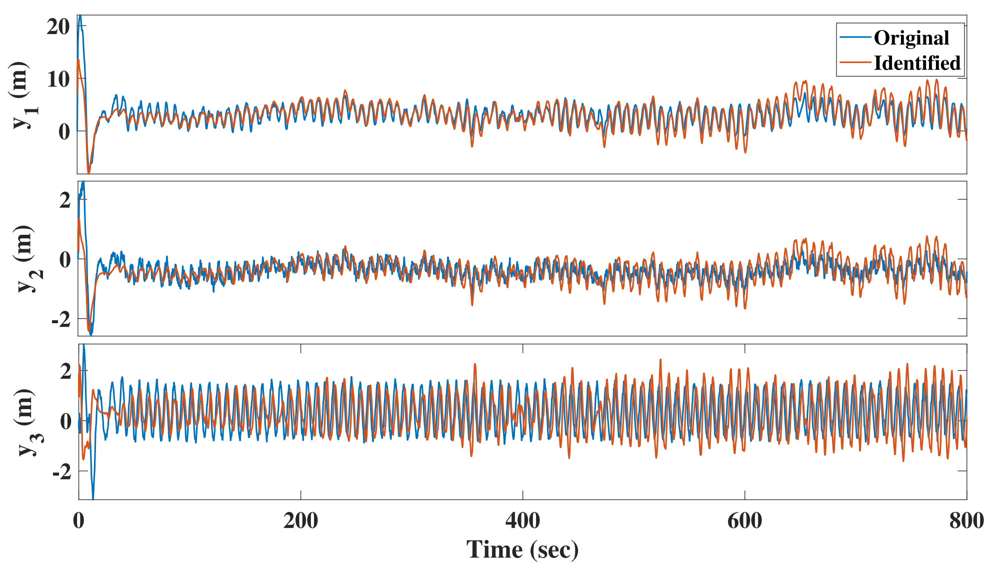

Fig. 4. Comparison of original (OpenFAST full-order simulation) and identified blade tip deformation of 15MW offshore wind turbine under turbulent wind conditions at 18.4197 m/s.

Table 1
Mean and standard deviations of blade tip deformation for the 15 MW offshore wind turbine across various wind conditions.

		12.4046 mps	15.2094 mps	18.4197 mps	20.2395 mps	23.9195 mps
	μ_1 (m)	9.8935	5.2740	4.2026	2.3114	1.2840
Mean	μ_2 (m)	1.0702	0.0093	−0.1708	−0.5386	−0.8982
	μ_3 (m)	0.4472	0.2904	0.2511	0.0245	−0.0875
	σ_1 (m)	2.6473	5.6249	6.6662	8.2085	8.7159
StandardDeviation	σ_2 (m)	0.4288	0.9135	1.1035	1.3536	1.5124
	σ_3 (m)	0.8286	0.9612	1.1211	1.2485	1.3216

of the desired responses. The Figs. 2, 3, 4, 5 and 6 compare the original and identified blade tip deformation of a 15 MW offshore wind turbine blade under different turbulent wind conditions: 12.4046 m/s, 15.2094 m/s, 18.4197 m/s, 20.2395 m/s and 23.9195 m/s, respectively. The blue lines referring to original responses from high-fidelity simulations, while the red lines shows the identified response obtained using the reduced-order state-space model with the ERA-OKID algorithm. In this comparison, the measurements y(i) correspond to the blade-tip deformation response time series extracted from the proposed model (refer Eq. (6)). This is an important parameter owing to the

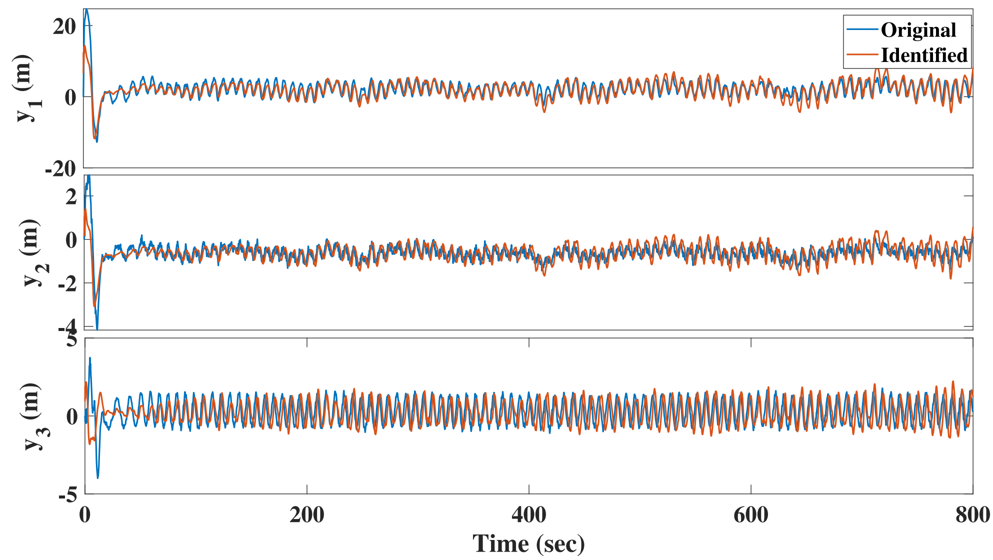

Fig. 5. Comparison of original (OpenFAST full-order simulation) and identified blade tip deformation of 15MW offshore wind turbine under turbulent wind conditions at 20.2395 m/s.

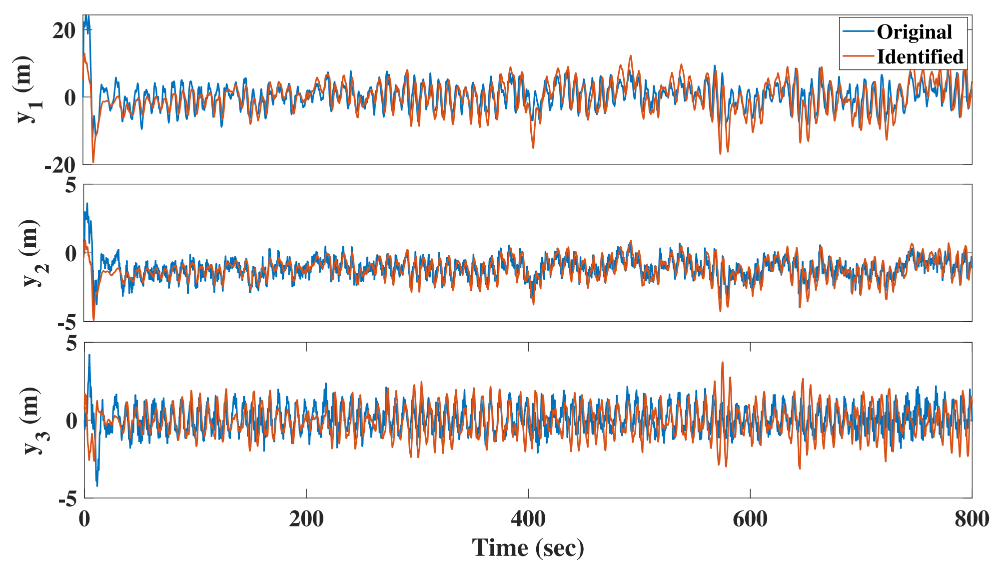

Fig. 6. Comparison of original (OpenFAST full-order simulation) and identified blade tip deformation of 15MW offshore wind turbine under turbulent wind conditions at 23.9195 m/s.

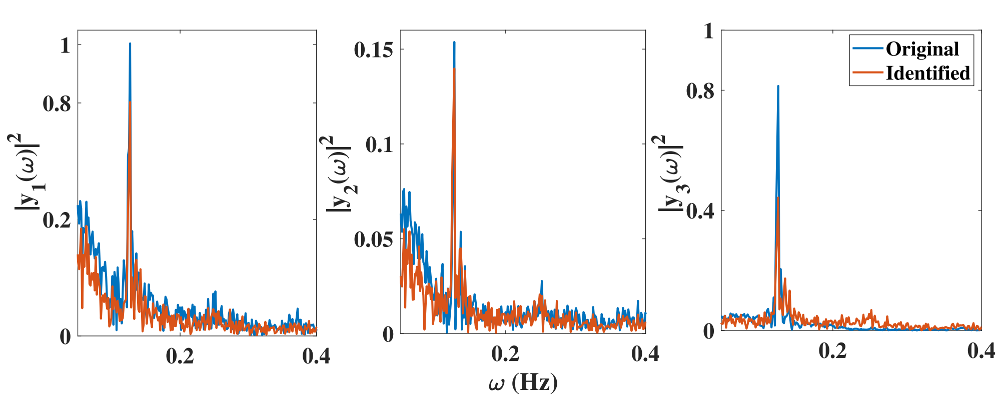

Fig. 7. Comparison of original (OpenFAST full-order simulation) and identified frequency domain responses of 15MW offshore wind turbine under turbulent wind conditions at 15.2094 m/s.

Table 2
Root mean square error (RMSE) between original and identified blade-tip deflections under turbulent inflow at five wind speeds.

Wind speed (m/s)	y_1 RMSE (m)	y_2 RMSE (m)	y_3 RMSE (m)
12.4046	0.55	0.18	0.22
15.2094	0.60	0.20	0.25
18.4197	0.32	0.15	0.22
20.2395	0.28	0.12	0.20
23.9195	0.35	0.18	0.25

fact that blade-tip deformation is directly linked to blade loading and fatigue; an accurate reduced-order model enables reliable blade-motion prediction and reconstruction from limited response channels and provides a control-ready model for feedback control aimed at vibration mitigation under turbulent inflow.

The consistency of these values, in totality, reinforces the efficacy and versatility of the reduced-order model for differing wind speeds and turbulence intensities. y_1, y_2 and y_3 are the first three modes of blade dynamics viz. two flapwise and one edgewise modes which are indicative of major vibrational characteristics of blades. The state-space model well predicts the overall dynamics of the wind turbine blade at all wind speeds. At lower wind speeds (i.e., 12.4046 m/s and 15.2094 m/s in Figs. 2 and 3), the identified blade tip deformation agree well with the original ones, especially in steady states. Very small differences in transient phases and peak values are found but they are tolerable for practical applications. This shows that the model is able to capture each of the three dominant mode of blade response during moderate turbulence conditions. As for the higher wind speed e.g. 18.4197 m/s, 20.2395 m/s and 23.9195 m/s (Figs. 4, 5 and 6), the differences between original and identified response becomes significant. At greater turbulence levels, for example, differences in amplitude and phase are clearly seen (as illustrated in y_1 and y_2) within the transient and oscillatory of the two modes. However, the third mode (y_3), which predominantly exhibits oscillatory behavior, remains well-captured across all wind speeds. The identified model effectively preserves the frequency and phase characteristics of this mode, though minor mismatches in amplitude, particularly during highly dynamic regions, suggest potential areas for improvement in capturing nonlinear effects and unsteady aerodynamic forces at elevated wind speeds. Comparison of the frequency domain responses of original and identified models under turbulent wind process at 15.2094 m/s is shown in Fig. 7. The results demonstrate that the identified model accurately captures the dominant frequencies and their respective amplitudes across all three modes (y_1, y_2, and y_3). There are subtle differences in the amplitudes for the higher harmonics, which can be attributed to modeling approximations and unsteady aerodynamic effects. Thus, the identified model shows good agreement with the original, particularly in capturing the primary frequency characteristics. To complement the frequency-domain agreement, we report the root-mean-square error (RMSE) as a time-domain, energy-equivalent measure of pointwise deviation over the full dataset. The discrepancy between the Original and Identified signals is quantified by the root-mean-square error (RMSE):

$$\mathrm{RMSE}(y_i) = \sqrt{\frac{1}{N}\sum_{k=1}^{N}\left(y_i^{\mathrm{o}}[k] - y_i^{\mathrm{id}}[k]\right)^2} \tag{43}$$

Table 2 reports the Root mean square error (RMSE) for the three outputs (y_1, y_2, y_3) at five wind speeds under turbulent inflow, summarizing the identification error used for ROM validation.

These results are of particular importance with respect to wind turbine control and monitoring. Reducing the three primary vibrational modes of the blade into a reduced-order state-space model, shows that high-fidelity dynamics can be accurately captured over a wide range of operating regimes. Thus, this model renders it an excellent fit for control applications, such as Model Predictive Control (MPC), where the model's computational efficiency and accuracy matter that most. Further, identification based on data from only the end node of a blade represents a practical feature of this proposed method owing to its less requirement while ensuring acceptable accuracy. This ensures that ERA-OKID can generate good control-oriented models of offshore wind turbines in turbulent winds that are more representative of real-world conditions.

5. Application of ERA-OKID model in model predictive control framework

Model Predictive Control (MPC) is an advanced optimal control strategy that leverages a system's predictive model to compute control inputs over a finite receding horizon by minimizing a cost function subject to dynamic and operational constraints. In the context of large-scale offshore wind turbines operating in turbulent environments, MPC provides a natural advantage in managing high-dimensional, coupled dynamics while accounting for input constraints and performance trade-offs.

The core of the MPC strategy employed here relies on a reduced-order model (ROM) constructed via the ERA-OKID technique. This technique extracts a discrete-time linear approximation of the system dynamics from measured input–output data, yielding the state-space model:

$$x_{k+1} = Ax_k + BF_k, \tag{44}$$

where $x_k \in \mathbb{R}^n$ is the state vector (e.g., nodal displacements and velocities of a blade tip), and F_k denotes the aerodynamic force input obtained as a nonlinear function of the blade pitch angle.

In this work, the Blade Element Momentum (BEM) loop is replaced by a physics-informed neural network (PINN) surrogate trained on data generated with a validated multi-body model of the IEA-15 MW turbine [7]. The network inputs are *measurable* quantities-blade pitch β, local axial/tangential inflow (V_x, V_y), and rotor speed ω-and the target is the angle of attack α at each blade node; sectional lift/drag and nodal loads are then reconstructed inside the controller, enabling the mapping

$$F_k = \mathcal{F}_{\mathrm{PINN}}\left(\beta_k, V_{x,k}, V_{y,k}, \omega_k\right). \tag{45}$$

Training data: Mean wind speeds from cut-in to cut-out were sampled via a Sobol sequence; for each mean speed, turbulent inflow was generated with two independent seeds. One seed was used for training and the other for validation, and mean speeds were also used to check cross-speed generalization. Tip and hub losses and yawed-inflow effects match those in the simulator. The PINN minimizes a composite loss

$$\mathcal{L} = \beta_m \mathcal{L}_{\mathrm{data}} + (1-\beta_m)\mathcal{L}_{\mathrm{phys}} + \lambda\|W\|_2^2, \tag{46}$$

blending data-fit error with a BEM residual, with mixing factor β_m and regularization λ selected by hyperparameter search. A fully connected feed-forward network with four hidden layers *using* tanh *activation functions* is trained with Adam, and inputs remain measurable to ensure controller compatibility. Across representative nodes the PINN attains $\mathrm{MAE}(\alpha) \sim 10^{-3} - 10^{-2}$ (i.e., $\lesssim 0.5°$), reconstructs loads within $\lesssim 5\%$ of BEM, and yields large wall-clock speed-ups when embedded in the MPC framework. At runtime, the surrogate uses only $(\beta, V_x, V_y, \omega)$, and all inputs required by the PINN are available within the MPC framework, supporting reliable closed-loop use.

The control objective is to determine the optimal pitch angle $\{\beta_k\}_{k=1}^{H_p}$ over a prediction horizon H_p that minimizes the cost:

$$\begin{aligned} J_{\mathrm{MPC}} \quad = \quad & \textstyle\sum_{k=1}^{H_p}\left[w_s \cdot x_k^\top x_k + w_p \cdot (P_{\mathrm{pred},k} - P_{\mathrm{ref},k})^2\right. \\ & \left. + w_r \cdot (\beta_k - \beta_{k-1})^2\right] \end{aligned} \tag{47}$$

where:

- w_s, w_p, w_r are scalar weights for state deviation, power tracking error, and pitch rate smoothness, respectively.

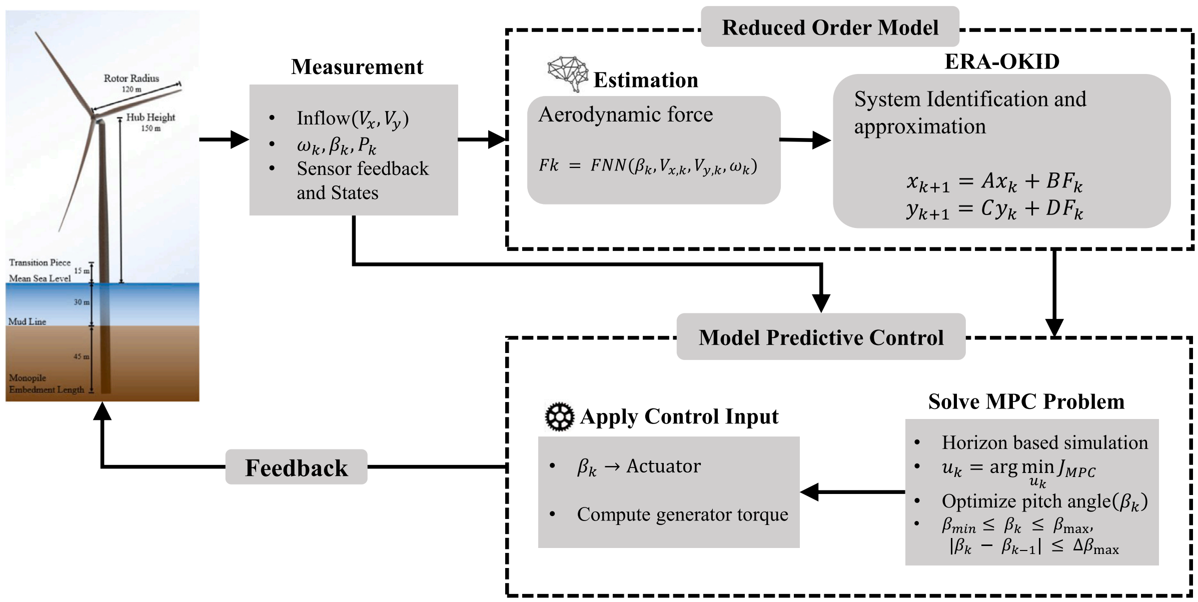

Fig. 8. Schematic of MPC-Driven Pitch Control using the ERA-OKID state space model.

- $P_{\text{pred},k} = T_{g,k} \cdot \omega_k$ is the predicted electrical power.
- $P_{\text{ref},k}$ is the reference power at step k, typically derived from a rated generator torque curve or operating strategy.

The pitch angles are bounded as:

$$\beta_{\min} \leq \beta_k \leq \beta_{\max}, \quad |\dot{\beta}_k| \leq \Delta\dot{\beta}_{\max}, \tag{48}$$

where β_k is the commanded collective pitch at time step k. In the simulations presented, we use $\beta_{\min} = 0\,rad$, $\beta_{\max} = 0.3491\,rad$ and $\dot{\beta}_{\max} = 0.0349\,rad/s$. The MPC loop is given in Algorithm 2 (see Fig. 8).

Algorithm 2 ERA-OKID based MPC for Wind Turbine Pitch Control

Input: Initial state x_0, initial pitch u_0, prediction horizon H_p, aerodynamic tables F_{table}, candidate pitch angles $\beta_{\text{candidates}}$

Initialize $x \leftarrow x_0$, $u_{\text{prev}} \leftarrow u_0$
for each control interval k **do**
  Predict aerodynamic force F_k using Eq. (45)
  Define cost function J_{MPC} based on Eq. (47)
  Obtain optimal pitch u_k
  Update state $x_{k+1} \leftarrow x_k + \Delta t(Ax_k + Bu_k)$
  Set $u_{\text{prev}} \leftarrow u_k$

The MPC framework, using by the ERA-OKID-based ROM and integrated neural force estimation, effectively captures essential turbine dynamics and ensures smooth pitch transitions. Time-domain simulations under turbulent wind inflow conditions demonstrate that the blade tip displacement remains bounded and exhibits no signs of dynamic instability or saturation, while pitch trajectories evolve smoothly within the imposed constraints. The approach enables pitch angle control of a 15MW offshore wind turbine, showcasing the potential of combining data-driven ROMs with physically interpretable force models within predictive control schemes. The present study focuses on the fixed-bottom monopile configuration under turbulent aerodynamic inflow. To isolate the wind-driven response and the effect of the proposed reduced-order model and control design, no wave excitation is applied. The MPC is implemented in discrete time with sampling period of 0.005s and a prediction horizon of 200 steps (1s). The average wall-clock computation time for the MPC optimization was 0.012394 s per control update (per sample), measured on a workstation with i7-12700H at 2.30 GHz and 32 GB RAM (64-bit OS).

5.1. Baseline controller used for benchmarking

We benchmark the proposed framework against the NREL Reference Open-Source Controller (ROSCO) implemented in OpenFAST through the ServoDyn user-defined controller interface (DISCON). ROSCO represents a widely used baseline for utility-scale turbines and comprises: (i) generator-speed filtering, (ii) multi-region variable-speed generator-torque control (Regions 1–3), and (iii) a gain-scheduled collective pitch PI controller with anti-windup and pitch-rate limits. Full implementation details are available in [30] and the ROSCO documentation.

(i) Generator-speed filtering. The measured generator speed ω_g is filtered by a first-order low-pass to remove high-frequency content:

$$\omega_g^f[k] = \alpha\,\omega_g^f[k-1] + (1-\alpha)\,\omega_g[k], \qquad \alpha = e^{-\omega_c T_s}, \tag{49}$$

where ω_c is the corner frequency and T_s is the sample period. The filtered speed ω_g^f is the sole feedback signal for both loops.

(ii) Variable-speed torque control (Regions 1–3). At each torque update (period T_{VS}), the commanded generator torque τ_g follows a standard multi-region law based on ω_g^f:

$$\tau_g(\omega_g^f) = \begin{cases} 0, & \omega_g^f \leq \omega_{\text{ci}} \quad \text{(Region 1)}, \\ m_{1.5}\,(\omega_g^f - \omega_{\text{ci}}), & \omega_{\text{ci}} < \omega_g^f < \omega_2 \quad \text{(Region 1.5)}, \\ K\,(\omega_g^f)^2, & \omega_2 \leq \omega_g^f < \omega_{\text{tr}} \quad \text{(Region 2)}, \\ m_{2.5}\,(\omega_g^f - \omega_{\text{syn}}), & \omega_{\text{tr}} \leq \omega_g^f < \omega_r \quad \text{(Region 2.5)}, \\ \dfrac{P_r}{\omega_g^f}, & \omega_g^f \geq \omega_r \quad \text{(Region 3, constant power)}. \end{cases} \tag{50}$$

(iii) Gain-scheduled collective-pitch PI. Pitch is updated every T_{PC} to regulate ω_g^f to ω_r. Let $e = \omega_g^f - \omega_r$ be the speed error and

$$G_K(\beta) = \frac{1}{1 + \beta/K_K} \tag{51}$$

be the pitch-dependent gain shaper. The PI law with anti-windup is

$$I \leftarrow \text{clip}\left(I + e\,T_{\text{PC}},\ \frac{\beta_{\min}}{G_K K_I},\ \frac{\beta_{\max}}{G_K K_I}\right), \tag{52}$$

$$\beta_c^\star = G_K(\beta)\left(K_P\,e + K_I\,I\right), \tag{53}$$

Table 3
Peak and root mean square (rms) of the controlled responses in turbulent conditions.

		Baseline		MPC		% Reduction	
		x_{peak} (m)	x_{rms} (m)	x_{peak} (m)	x_{rms} (m)	x_{peak} (m)	x_{rms} (m)
Turbulence intensity 10%	12.4 m/s	13.956	7.26	13.20	6.78	5.42	6.61
	15.2 m/s	12.98	6.78	10.85	5.19	16.41	23.45
Turbulence intensity 14%	12.4 m/s	14.046	9.923	11.78	8.263	15.67	16.73
	15.2 m/s	12.37	6.19	8.24	4.18	33.4	32.31
Turbulence intensity 18%	12.4 m/s	14.96	6.40	12.46	5.76	16.71	10.00
	15.2 m/s	11.18	6.61	9.51	4.78	14.94	27.69

$$\beta_c = \mathrm{clip}\left(\beta_c^\star,\ \beta_{\min},\ \beta_{\max}\right), \tag{54}$$

where (K_P, K_I) are the PI gains and $[\beta_{\min}, \beta_{\max}]$ are the physical limits. The commanded change is rate-limited on each blade and applied collectively:

$$\dot{\beta} = \mathrm{clip}\left(\frac{\beta_c - \beta}{T_{\mathrm{PC}}},\ -\dot{\beta}_{\max},\ \dot{\beta}_{\max}\right), \qquad \beta \leftarrow \beta + \dot{\beta}\, T_{\mathrm{PC}} \tag{55}$$

Using the same measurements, sampling times, physical limits, and rate limits for both controllers ensures a fair comparison; therefore, the improvements reported for ROM-MPC (reduced loads and lower pitch activity) can be attributed to the identified model and MPC formulation rather than to differences in baseline tuning or constraints.

5.2. Results and discussion

To assess the accuracy of the ERA-OKID based ROM for control purposes, we integrated it with a Model Predictive Control (MPC) framework aimed at the control of blade pitch for a 15MW offshore wind turbine model. Fig. 8 illustrates the closed-loop framework of the wind turbine pitch control system, integrating ERA-OKID-based reduced-order modeling, and MPC design. The purpose of this section is to verify that the ERA-OKID-identified model supports stable and feasible control behavior under realistic aerodynamic loading conditions. Performance of wind turbine were represented by timeseries simulations under above-rated wind speed conditions. The prediction for the MPC scheme was based on the ERA-OKID state-space matrices (A, B) and a NN model [7] was used to transform blade pitch angles into nodal loads. The simulation is carried out under above-rated wind conditions 12.4 m/s and 15.2 m/s for three levels of turbulence intensity.

The rotor average wind excitation and corresponding out-of-plane blade tip deflection for one of the blades is depicted in Fig. 9 and Fig. 10 respectively. The response is steady for the duration of the simulation, with vibration levels consistent with expected dynamic behavior of the turbine under turbulent wind. The pitch controller reacts slowly to changes in aerodynamic conditions, and there is very less structural dynamic instability or drift observed in contrast with the baseline controller. This shows the capability of ERA-OKID model to captures sufficient dynamics for vibration-based pitch control. Similarly, Fig. 11 presents the corresponding blade pitch angle trajectory juxtaposed with the . The smoother pitch activity observed in the results follows from the optimization-based control formulation, while the imposed hard bounds ensure that the commanded pitch remains within actuator-safe limits. Finally Fig. 12 compares the electrical power output for the tested above-rated turbulent case. The MPC generally provides smoother pitch activity and competitive power regulation relative to the baseline. Its benefit is more evident when the wind fluctuations are stronger, whereas during temporary reductions toward rated or slightly below-rated conditions the difference between the two controllers becomes less pronounced. Table 3 presents the peak and root mean square (rms) of the out-of-plane blade tip deflection, and Table 4 presents the standard deviation and mean rate of the pitch angle under three turbulent wind conditions across two above-rated wind speeds. The MPC controller was identified and optimized for a nominal wind speed of 12.4 m/s, and shows its greatest effectiveness at or near this wind speed.

The MPC controller was identified and optimized for a nominal wind speed of 12.4 m/s and shows its strongest benefit at or near this operating point. Across the tested above-rated turbulent conditions, the controller reduces blade-tip deflection and pitch-actuation measures relative to the baseline, with the clearest improvements observed under higher turbulence. Specifically, the blade tip deflection is significantly reduced, with peak and rms values reduced by up to 17% and 28%, respectively. Similarly, the pitch actuation efforts are substantially lowered: the standard deviation and mean rate of pitch angle are reduced by over 60% in most of the tested cases, reaching up to 92.58% and 86.15% reduction, respectively, at 12.4 m/s and 14% turbulence intensity. At operating points farther from the identification condition, or when wind-speed dips are less pronounced, the performance advantage becomes more modest. These results therefore support the use of the proposed controller particularly for above-rated and more turbulent operating conditions, rather than implying uniform superiority across all regimes.

These reductions indicate that the MPC controller not only effectively mitigates structural loads but also smooths pitch actuator behavior, which is crucial for reducing fatigue and extending turbine lifespan. Even at mean wind speeds away from the identification point such as 15.2 m/s with large turbulence intensity such as 18%, the controller continues to offer meaningful reductions in both blade loads and actuation effort, demonstrating strong generalization capability. The numerical results demonstrate that the ERA-OKID model provides a practical and reliable basis for model-based control design. The MPC implementation confirms that the reduced-order representation derived via ERA-OKID enables real-time pitch regulation that respects turbine limits, while achieving desirable closed-loop dynamic response. These findings support the viability of ERA-OKID modeling for advanced wind turbine control applications.

Across the turbulent scenarios considered here, the proposed controller reduces blade tip–deflection RMS by 10%–28% (and peaks by 2%–17%) while mean pitch-rate decreases by 59%–93% and pitch-angle σ by 41%–86% (Tables 2–3). These outcomes are consistent with recent output-constrained individual pitch control (IPC) results that explicitly map the trade-off between damage-equivalent load (DEL) and actuator duty cycle (ADC) on the IEA-15 MW turbine: one operating point achieves 50% DEL reduction with only 16.4% of the actuator duty of full IPC (same crossover frequency), and under turbulent inflow 87% of full-IPC load reduction at 50% of the actuation [27]. Similarly, constrained subspace predictive repetitive control (cSPRC) on the 10 MW reports 25% blade-load reduction at 4% actuator duty, emphasizing low-duty operation by activating only when loads exceed bounds [28]. Full-scale field data further point the same way: an MPC system on a 3-MW turbine reduced power-fluctuation Interquartile range (IQR) by 25% and tower-mode amplification by 80% relative to a baseline proportional integral derivative (PID) controller [38].

The additional wind-pitch and wind-power comparisons in Figs. 13 and 14 further clarify the controller behavior during temporary wind-speed reductions. In particular, when the average wind speed falls toward or slightly below the rated value, the baseline pitch controller tends to drive the blade pitch close to zero, which is consistent with conventional gain-scheduled operation in the below-rated region. By contrast, the proposed MPC does not always return the pitch angle fully

Table 4
Standard deviation and mean rate of the pitch angle in turbulent condition.

		Baseline		MPC		% Reduction	
		β_{std} (rad)	$\dot{\beta}_{mean}$ (rad/s)	β_{std} (rad)	$\dot{\beta}_{mean}$ (rad/s)	β_{std} (rad)	$\dot{\beta}_{mean}$ (rad/s)
Turbulence intensity 10%	12.4 m/s	0.0425	0.0026	0.0089	0.00056	79.05	78.46
	15.2 m/s	0.0489	0.0024	0.0221	0.00062	54.81	74.16
Turbulence intensity 14%	12.4 m/s	0.0491	0.0031	0.0058	0.00023	86.15	92.58
	15.2 m/s	0.0436	0.002	0.0241	0.00062	44.72	69.00
Turbulence intensity 18%	12.4 m/s	0.0443	0.0031	0.0156	0.00072	10.00	76.77
	15.2 m/s	0.0522	0.002	0.0572	0.00082	27.69	59.00

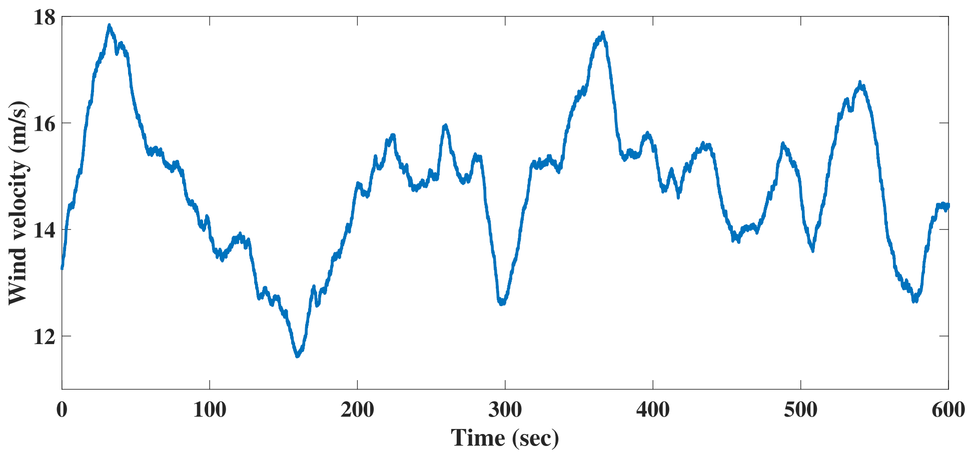

Fig. 9. Rotor average wind excitation time history for 15MW offshore wind turbine with mean wind speed 15.2 m/s under turbulence intensity 14%.

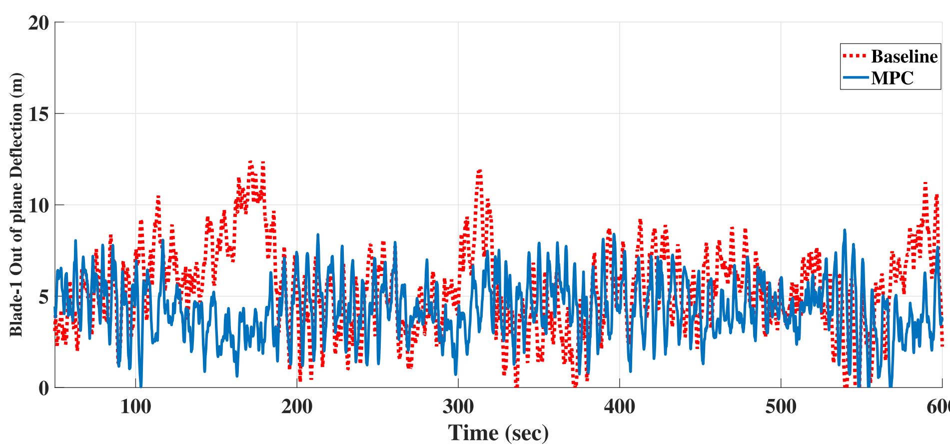

Fig. 10. Comparison of out-of-plane blade tip deflection for 15MW offshore wind turbine with mean wind speed 15.2 m/s under turbulence intensity 14%.

to zero during such short duration dips. This is because the MPC is formulated around above-rated operation and optimizes a constrained finite-horizon objective that balances power regulation, pitch activity, and actuator usage. As a result, for brief excursions of wind speed below rated, it can be optimal to retain a nonzero pitch bias rather than command a rapid transition to zero pitch followed by an equally rapid re-pitching action when the wind recovers. This behavior reflects the intended trade-off between regulation quality and actuator effort, and is consistent with the smoother pitch activity observed in Fig. 13 while preserving satisfactory power output in Fig. 14.

This study targets controller-ready, low-overhead modeling and control. The ERA–OKID model is identified from a single input–output dataset, retains a linear state-space form suitable for MPC/LQR, and in our tests generalizes across wind speeds without re-identification. These features complement (rather than replace) other strands: operational modal analysis (OMA) and linear parameter-varying (LPV) identification is well-suited to blade-periodic regimes [25]; surrogate aerodynamic models based on PINNs can bypass BEM iterations and accelerate load prediction but generally require additional steps for direct controller [7].

6. Conclusions

This work presents a novel control-oriented modeling and optimization framework that uses the ERA-OKID algorithm to form a reduced-order state-space model of wind turbine blade dynamics, to be used within a Model Predictive Control (MPC) framework for pitch angle control. The proposed model accurately captures key dynamic behaviors by representing two flapwise and one edgewise vibrational modes using a single input–output dataset. Aerodynamic loads are incorporated through modal forcing derived from PINN surrogate modeling, enabling a compact yet physically representative model suitable for control applications. The novelty of this approach lies not only in the minimal data requirements for model identification but also in

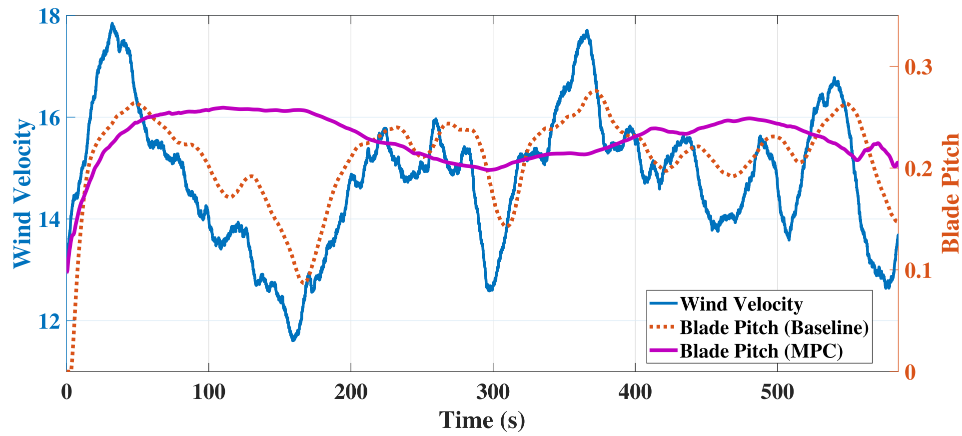

Fig. 11. Comparison of pitch angle (right axis) for 15MW offshore wind turbine with mean wind speed 15.2 m/s under turbulence intensity 14% (left axis).

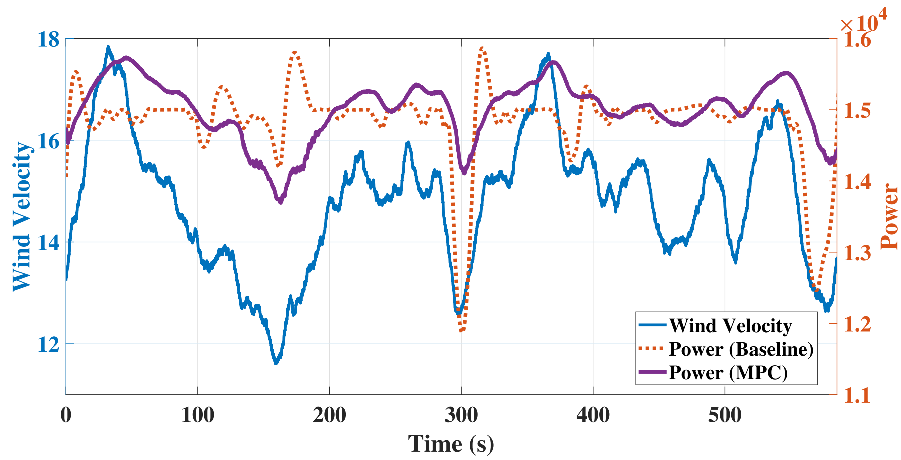

Fig. 12. Comparison of Power (right axis) for 15MW offshore wind turbine with mean wind speed 15.2 m/s under turbulence intensity 14% (left axis).

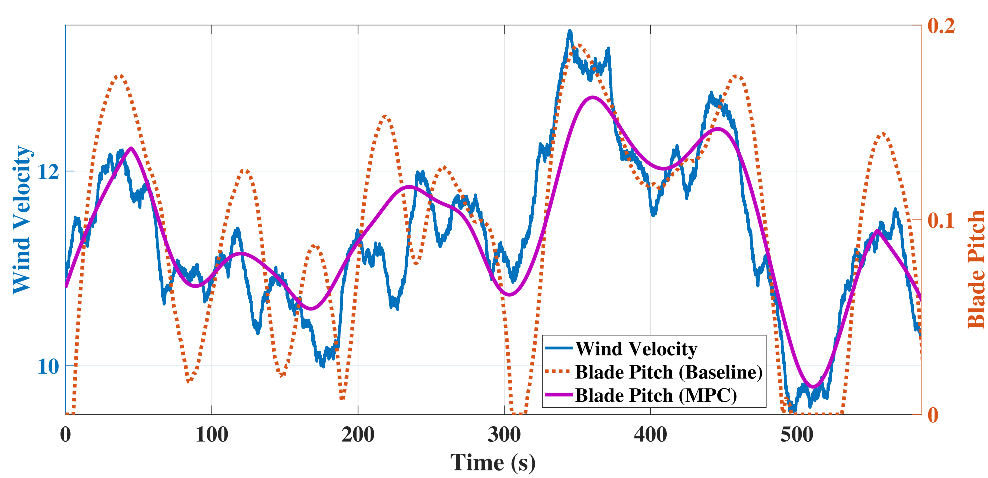

Fig. 13. Comparison of pitch angle (right axis) for 15MW offshore wind turbine with mean wind speed 12.4 m/s under turbulence intensity 10% (left axis).

its capability to enable advanced-control strategies without relying on full-order aeroelastic simulations. The integration of this reduced-order model into an MPC framework allows for constraint-aware, anticipatory pitch control that actively reduces structural vibration with less actuation.

In the tested above-rated turbulent scenarios, the proposed ERA-OKID–MPC framework reduced RMS blade-tip deflection by up to 28% and mean pitch-rate by up to 93% relative to the baseline controller. The strongest benefits were observed near the nominal identification condition and under more turbulent inflow, where smoother pitch activity translated into clearer load-mitigation advantages. Under lower-wind or less demanding conditions, the improvement over the baseline is more limited. Therefore, the present results support the proposed approach as a promising controller-ready framework particularly

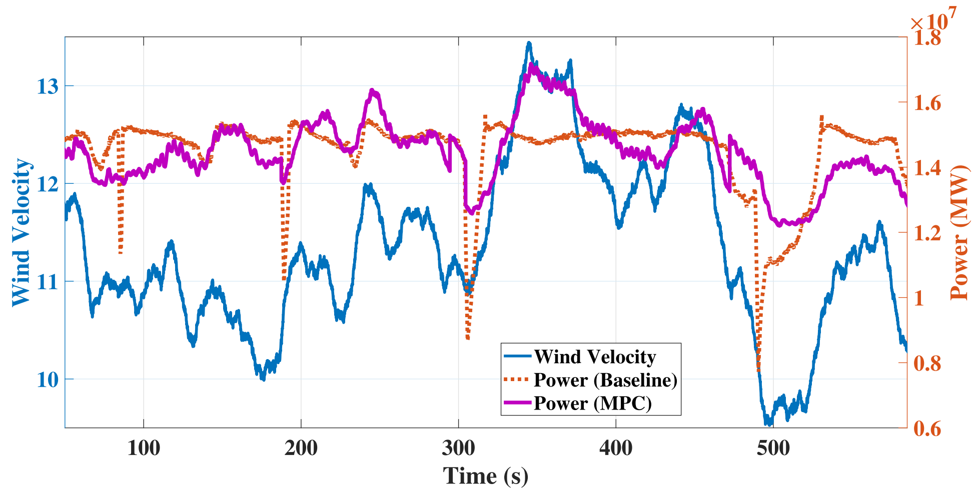

Fig. 14. Comparison of Power (right axis) for 15MW offshore wind turbine with mean wind speed 12.4 m/s under turbulence intensity 10% (left axis).

for above-rated and more turbulent operating regimes, while broader validation across all operating regions remains future work.

CRediT authorship contribution statement

Satyam Panda: Writing – original draft, Software, Methodology, Investigation, Formal analysis, Data curation, Conceptualization. **Shubham Baisthakur:** Writing – review & editing, Software, Methodology, Data curation, Conceptualization. **Hamid Reza Karimi:** Writing – review & editing, Methodology, Conceptualization. **Breiffni Fitzgerald:** Writing – review & editing, Supervision, Methodology, Investigation, Funding acquisition, Conceptualization.

Declaration of competing interest

The authors declare that they have no known competing financial interests or personal relationships that could have appeared to influence the work reported in this paper.

Acknowledgments

This work is supported by Science Foundation Ireland (SFI) grant no. 20/FFP-P/8702, and SFI project NexSys, Ireland grant no. 21/SPP/3756.

Data availability

The data presented in this study are available on request from the corresponding author. The data are not publicly available because it also forms part of an ongoing study.

References

[1] Wadim Strielkowski, Evgeny Lisin, Inna Gryshova, Climate policy of the European union: What to expect from the Paris agreement, Rom. J. Eur. Aff. 16 (2016) 68.
[2] M Dolores Esteban, J Javier Diez, Jose S López, Vicente Negro, Why offshore wind energy? Renew. Energy 36 (2) (2011) 444–450.
[3] Paul Veers, Carlo L Bottasso, Lance Manuel, Jonathan Naughton, Lucy Pao, Joshua Paquette, Amy Robertson, Michael Robinson, Shreyas Ananthan, Thanasis Barlas, et al., Grand challenges in the design, manufacture, and operation of future wind turbine systems, Wind. Energy Sci. 8 (7) (2023) 1071–1131.
[4] Xu Zhang, Lijun Zhang, Kaifei Wang, Xudong Cui, Ziyi Liu, Zhengjun Jing, Shibo Liu, Jiahui Lu, Baoping Cai, Aerodynamic-structural similarity criteria for scaled-down models of ultra-long wind turbine blade, Renew. Energy (2025) 124184.
[5] Sourav Das, M. Mohamed Sajeer, Arunasis Chakraborty, Vibration control of horizontal axis offshore wind turbine blade using SMA stiffener, Smart Mater. Struct. 28 (9) (2019) 095025.
[6] Hamid Khakpour Nejadkhaki, John F Hall, Minghui Zheng, Teng Wu, Integrative modeling platform for design and control of an adaptive wind turbine blade, in: Dynamic Systems and Control Conference, vol. 51906, American Society of Mechanical Engineers, 2018, V002T28A005.
[7] Shubham Baisthakur, Breiffni Fitzgerald, Physics-informed neural network surrogate model for bypassing blade element momentum theory in wind turbine aerodynamic load estimation, Renew. Energy 224 (2024) 120122.
[8] Liang Li, Yuanchuan Liu, Zhiming Yuan, Yan Gao, Dynamic and structural performances of offshore floating wind turbines in turbulent wind flow, Ocean Eng. 179 (2019) 92–103.
[9] Shubham Baisthakur, Vikram Pakrashi, Subhamoy Bhattacharya, Breiffni Fitzgerald, Impact of sources of damping on the fragility estimates of wind turbine towers, ASCE-ASME J. Risk Uncertain. Eng. Syst. Part B: Mech. Eng. 10 (4) (2024) 041202.
[10] Kyungil Kong, Kirsten Dyer, Christopher Payne, Ian Hamerton, Paul M Weaver, Progress and trends in damage detection methods, maintenance, and data-driven monitoring of wind turbine blades–a review, Renew. Energy Focus. 44 (2023) 390–412.
[11] Ziqian Kong, Baoping Tang, Lei Deng, Wenyi Liu, Yan Han, Condition monitoring of wind turbines based on spatio-temporal fusion of SCADA data by convolutional neural networks and gated recurrent units, Renew. Energy 146 (2020) 760–768.
[12] Davide Selvatici, Richard JAM Stevens, Capturing tip-corrected blade element momentum loading with wind turbine models, Renew. Energy 241 (2025) 122265.
[13] Qian Zhang, S. Khaitan, J. McCalley, V. Ajjarapu, MIMO system identification for large power systems preserving dominant oscillatory dynamics, in: 2018 IEEE Power & Energy Society General Meeting, PESGM, 2018, pp. 1–5.
[14] A. Cezayirli, M.K. Ciliz, Indirect adaptive control of non-linear systems using multiple identification models and switching, Internat. J. Control 81 (2008) 1434–1450, http://dx.doi.org/10.1080/00207170701837371.
[15] Bart Peeters, Guido De Roeck, Stochastic system identification for operational modal analysis: a review, J. Dyn. Sys. Meas. Control. 123 (4) (2001) 659–667.
[16] Adrian Stetco, F. Dinmohammadi, Xingyu Zhao, V. Robu, D. Flynn, M. Barnes, J. Keane, G. Nenadic, Machine learning methods for wind turbine condition monitoring: A review, Renew. Energy (2019) http://dx.doi.org/10.1016/J.RENENE.2018.10.047.
[17] A. Palmeri, A state-space viscoelastic model of double-beam systems toward the dynamic analysis of wind turbine blades, in: Earth and Space 2010: Engineering, Science, Construction, and Operations in Challenging Environments, 2010, pp. 1973–1980.
[18] Lijuan Liu, Feng Ding, Ling Xu, Jian Pan, Ahmed Alsaedi, Tasawar Hayat, Maximum likelihood recursive identification for the multivariate equation-error autoregressive moving average systems using the data filtering, IEEE Access 7 (2019) 41154–41163.
[19] B.L. Ho, Rudolf E. Kálmán, Effective construction of linear state-variable models from input/output functions: Die konstruktion von linearen modeilen in der darstellung durch zustandsvariable aus den beziehungen für ein-und ausgangsgrößen, At-Automatisierungstechnik 14 (1–12) (1966) 545–548.
[20] Samet Oymak, Necmiye Ozay, Revisiting ho–kalman-based system identification: Robustness and finite-sample analysis, IEEE Trans. Autom. Control 67 (4) (2021) 1914–1928.
[21] Elvio Bonisoli, Alessandro Fasana, Luigi Garibaldi, Stefano Marchesiello, Donato Sabia, Advances in identification and fault detection in bridge structures, Key Eng. Mater. 245 (2003) 339–350.

[22] Aoife Henry, Manuel Pusch, Lucy Pao, Investigation of $H\infty$-tuned individual pitch control for wind turbines, Wind. Energy 27 (10) (2024) e2945.

[23] Yuan-Zhuo Ma, Jia Wei, Wei-Dong Liu, Peng-Peng Zhi, Zhen-Zhou Zhao, Chang Xu, Hong-Shuang Li, Design optimization of composite wind turbine blade using complete constrained expected improvement-subset simulation optimization, Renew. Energy (2025) 123187.

[24] Jer-Nan Juang, Richard S. Pappa, An eigensystem realization algorithm for modal parameter identification and model reduction, J. Guid. Control Dyn. 8 (5) (1985) 620–627.

[25] Aemilius AW van Vondelen, Sachin T Navalkar, Alexandros Iliopoulos, Daan C van der Hoek, Jan-Willem van Wingerden, Damping identification of offshore wind turbines using operational modal analysis: a review, Wind. Energy Sci. 7 (1) (2022) 161–184.

[26] Gunjit Bir, Multi-blade coordinate transformation and its application to wind turbine analysis, in: 46th AIAA Aerospace Sciences Meeting and Exhibit, 2008, p. 1300.

[27] Jesse Ishi Storm Hummel, Jens Kober, Sebastiaan Paul Mulders, Output-constrained individual pitch control methods using the multiblade coordinate transformation: Trading off actuation effort and blade fatigue load reduction for wind turbines, Wind. Energy Sci. Discuss. 2025 (2025) 1–31.

[28] Yichao Liu, Riccardo Ferrari, Jan-Willem van Wingerden, Load reduction for wind turbines: an output constrained, subspace predictive repetitive control approach, Wind. Energy Sci. Discuss. 2021 (2021) 1–23.

[29] Nikhar J. Abbas, Alan Wright, Lucy Pao, An Update to the NREL Baseline Wind Turbine Controller Preprint.

[30] Nikhar J. Abbas, Daniel S. Zalkind, Lucy Pao, Alan Wright, A reference open-source controller for fixed and floating offshore wind turbines, Wind. Energy Sci. 7 (1) (2022) 53–73.

[31] Mohammad J Yarmohammadi, Arash Sadeghzadeh, Mostafa Taghizadeh, Gain-scheduled control of wind turbine exploiting inexact wind speed measurement for full operating range, Renew. Energy 149 (2020) 890–901.

[32] Evan Gaertner, Jennifer Rinker, Latha Sethuraman, Frederik Zahle, Benjamin Anderson, Garrett Barter, Nikhar Abbas, Fanzhong Meng, Pietro Bortolotti, Witold Skrzypinski, George Scott, Roland Feil, Henrik Bredmose, Katherine Dykes, Matt Sheilds, Christopher Allen, Anthony Viselli, Definition of the IEA 15-Megawatt Offshore Reference Wind Turbine, Technical report, International Energy Agency, 2020, URL https://www.nrel.gov/docs/fy20osti/75698.pdf.

[33] Thomas R. Kane, David A. Levinson, Dynamics, Theory and Applications, McGraw Hill, 1985.

[34] G. Bir, User's Guide to Bmodes (Software for Computing Rotating Beam-Coupled Modes), Technical report, National Renewable Energy Lab.(NREL), Golden, CO (United States), 2005.

[35] R.S. Sengar, K. Chatterjee, J. Singh, System approximation via restructured Hankel matrix, Circuits Systems Signal Process. 40 (2021) 6354–6370, http://dx.doi.org/10.1007/s00034-021-01745-2.

[36] B. Peeters, G. Roeck, Reference-based stochastic subspace identification for output-only modal analysis, Mech. Syst. Signal Process. 13 (1999) 855–878, http://dx.doi.org/10.1006/MSSP.1999.1249.

[37] A. Alenany, D. Westwick, H. Shang, A modified observer/Kalman filter identification (OKID) algorithm employing output residuals, Int. J. Dyn. Control. 7 (2019) 636–643, http://dx.doi.org/10.1007/S40435-018-00502-9.

[38] Sebastian Dickler, Thorben Wintermeyer-Kallen, János Zierath, Reik Bockhahn, Dirk Machost, Thomas Konrad, Dirk Abel, Full-scale field test of a model predictive control system for a 3 mw wind turbine, Forsch. Im Ingenieurwesen 85 (2) (2021) 313–323.